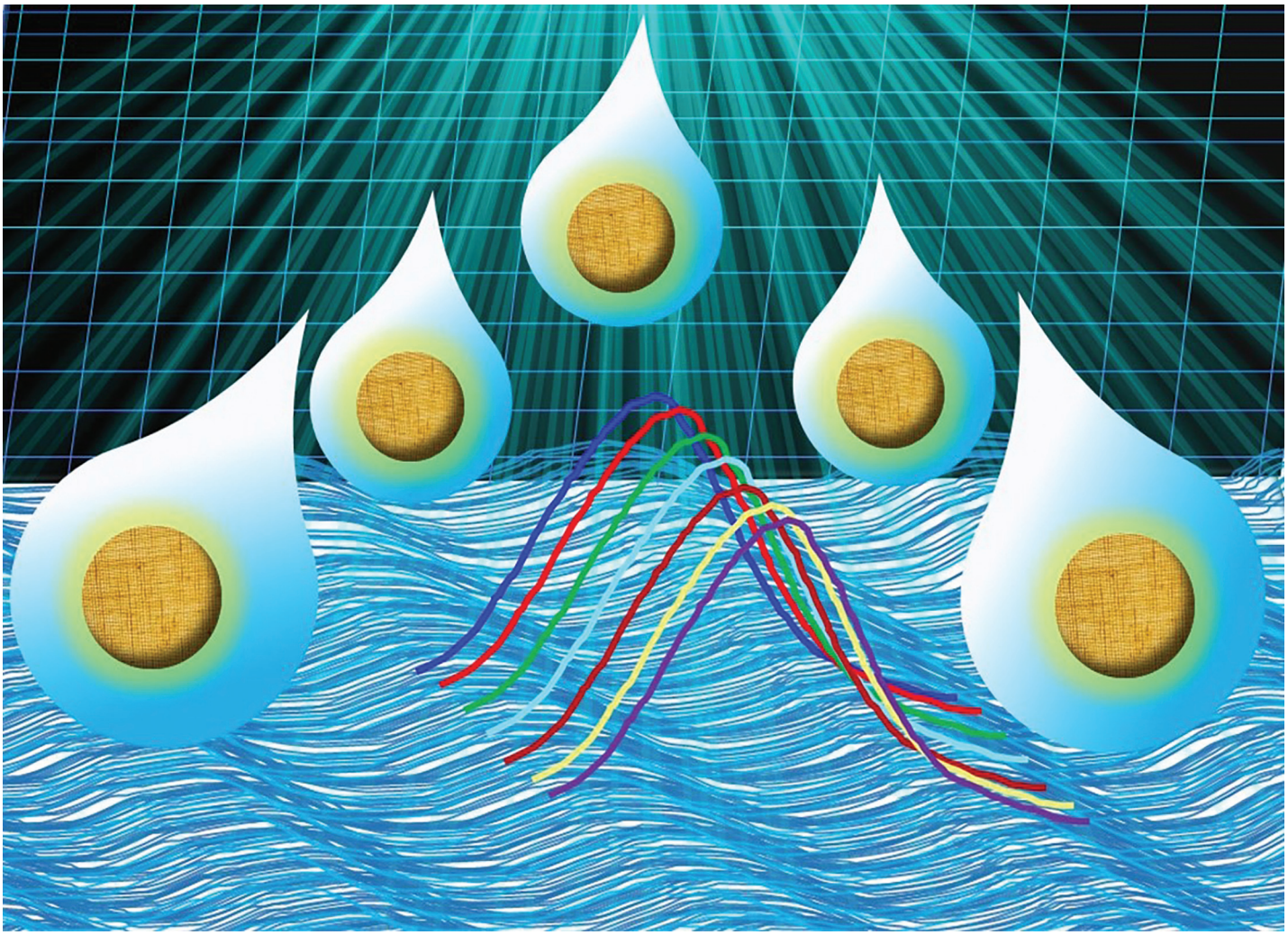

Featuring the research work of Soumen Ghosh and co-workers from the Macromolecular Chemistry and Engineering Research (MCER) Group, led by Dr Subrata Chattopadhyay at Department of Chemistry, Indian Institute of Technology Patna.

Stimuli-directed selective detection of Cu^{2+} and $Cr_2O_7^{2-}$ ions using a pH-responsive chitosan-poly(aminoamide) fluorescent microgel in aqueous media

This work demonstrates the development of chitosan-polyaminoamide fluorescent microgels for highly selective detection of both Cu^{2+} and $Cr_2O_7^{2-}$ in water.

As featured in:

See Subrata Chattopadhyay *et al.*, *Soft Matter*, 2024, **20**, 79.

ROYAL SOCIETY OF CHEMISTRY

rsc.li/soft-matter-journal

Registered charity number: 207890

Soft Matter

PAPER

View Article Online
View Journal | View Issue

Check for updates

Cite this: *Soft Matter*, 2024, **20**, 79

Stimuli-directed selective detection of Cu^{2+} and $Cr_2O_7^{2-}$ ions using a pH-responsive chitosan-poly(aminoamide) fluorescent microgel in aqueous media†

Soumen Ghosh, Jyoti Devi Katiyar and Subrata Chattopadhyay *

Received 3rd October 2023,
Accepted 11th November 2023

DOI: 10.1039/d3sm01319g

rsc.li/soft-matter-journal

In this work, the preparation of a pH-responsive fluorescent microgel, (NANO-PAMAM-CHT), is presented for the selective detection of Cu^{2+} and $Cr_2O_7^{2-}$ ions. The NANO-PAMAM-CHT (nanosized polyaminoamide-chitosan microgel) is synthesized *via* aza-Michael addition reactions in a controlled and stepwise manner in water, using easily affordable starting materials like 1,4-diaminobutane, *N*,*N*′-methylene-bis-acrylamide, NIPAM and chitosan. NANO-PAMAM-CHT shows pH-responsive fluorescent properties, whereas the fluorescence intensity shows a pH-responsive change. Due to the selective fluorescence quenching, the microgel can detect both Cu^{2+} ions and $Cr_2O_7^{2-}$ ions selectively at ambient pH in aqueous medium. Moreover, it can selectively differentiate between Cu^{2+} ion and $Cr_2O_7^{2-}$ ions at pH ∼3 in water. The limits of detection for Cu^{2+} ions and $Cr_2O_7^{2-}$ ions are reported as 16.9 μM and 2.62 μM, respectively (lower than the minimum allowed level in drinking water) at pH ∼7. Mechanistic study further reveals the dynamic quenching phenomenon in the presence of Cu^{2+} ions and static quenching in the presence of $Cr_2O_7^{2-}$ ions.

Introduction

With the exponential growth of different chemical industries and unethical waste disposal practices, water pollution has emerged as a global issue.[1–3] Therefore, simple and affordable detection of toxic components is extremely important and has emerged as a fascinating research area due to their chemical[4,5] and biological[6,7] applications. In this context, colorimetric and fluorescent sensors have attracted much more attention because of their selectivity, high sensitivity, low cost, and fast response time for the detection of cationic and anionic species.[8–11] Without the help of highly expensive instruments like atomic absorption spectroscopy (AAS), and inductively coupled plasma-mass spectrometry (ICP-MS), the fluorescence-sensor based metal ion detection technique is a straightforward and low-cost process and therefore, the development of such sensors has attracted much attention.[12,13] In this context, several advanced functional materials such as carbon dots,[14,15] quantum dots,[16,17] metal ion based fluorophores,[18–20] polymers,[21–25] small molecular organic probes,[26–28] micelles[29] and microgels[30,31] are reported. In most of the cases, such fluorophores can selectively detect a single ion.[19,32] However, this limits its practical applicability to an extent, and therefore recent efforts are going towards the detection of more than one ion selectively using a single fluorescent probe. In this context, a few conjugated hydrophobic organic and polymeric fluorophores are reported which can detect more than one metal ion by varying the solvent systems or the ratio of organic to aqueous mixtures.[33–35] Besides, a few metal organic framework-based fluorophores have demonstrated the detection of more than one metal ion; however, most of them suffer from less or no selectivity between the detectable analytes.[16,36,37] In addition, metal organic framework-based sensors generally suffer from low water stability and solubility, which limits their practical applicability for detection.[38,39] Therefore, stimuli responsive polymer materials, such as microgels can be a better choice due to their smart responsive properties and higher water stability. Examples of fluorescent microgels are already known, which have demonstrated their ability to detect metal ions in aqueous solution.[30,40,41] In the majority of these reports, it demonstrated selective detection of single metal ions under ambient temperature and pH. Recently, Dong *et al.* reported a responsive microgel for the selective detection of Fe^{3+} and Mn^{2+} at pH ∼2 and pH ∼12, respectively.[30] However, no detection is possible at ambient pH and also the performance is effected by a change of temperature.

Department of Chemistry, Indian Institute of Technology Patna, Bihta, Patna 801106, Bihar, India. E-mail: sch@iitp.ac.in

† Electronic supplementary information (ESI) available. See DOI: https://doi.org/10.1039/d3sm01319g

Published on 13 November 2023. Downloaded on 07/09/2025 11:09:43 PM.

Published on 13 November 2023. Downloaded on 07/09/2025 11:09:43 PM.

Herein, we are aiming to develop a stimuli-responsive fluorescent microgel as a single fluorescent probe, which can sense both Cu^{2+} ions and $Cr_2O_7^{2-}$ ions selectively in aqueous solution. Both the analytes are marked as priority pollutants by the United States Environmental Protection Agency.[42] The third most abundant transition metal in human bodies is Cu^{2+}, among all the transition metal ions. Towards living organisms, Cu^{2+} becomes a hazardous and toxic element at high concentration.[42] Neurodegenerative disorders, such as Alzheimer's disease, Wilson's disease and Menkes disease, are associated with the unregulation of the Cu^{2+} ion.[43] According to the US Environmental Protection Agency (EPA), the limit for copper is 20 μM in drinking water.[42] Besides, the dichromate ion ($Cr_2O_7^{2-}$) is known to be extremely toxic for all living beinga.[44] Even at a very low concentration, dichromate can lead to serious health issues, like damage to the mucus membrane, lung cancer, renal damage, pulmonary sensitivity, targeting the respiratory tract and damaging the skin.[45] According to the American Water Works Association: Denver, CO, USA, the maximum allowed contaminant level of dichromate ions is 5 μM.[46] Therefore, selective detection of these two ions is important.

In the present work, we have designed and developed a stimuli responsive microgel (NANO-PAMAM-CHT) for the selective detection of two different ions in aqueous media with the variation of the pH. The microgel core backbone is comprised of polyaminoamide, a nonconventional hydrophilic fluorescent polymer, which is modified with chitosan to prepare NANO-PAMAM-CHT (nanosized polyaminoamide-chitosan microgel). Chitosan is a biobased polymer, containing amines and hydroxyl groups, which can interact with different metal ions and is therefore useful for metal ion sensing.[47] Besides, for the current system, the primary amine groups of chitosan can act as a binding site (Michael-donor) to react with the acrylamide moieties (Michael-acceptor) of NANO-PAMAM. NANO-PAMAM-CHT can selectively detect both Cu^{2+} and $Cr_2O_7^{2-}$ at ambient pH and temperature. Besides, the pH-responsive property of NANO-PAMAM-CHT further discriminates between the two detected ions (Cu^{2+} ion from $Cr_2O_7^{2-}$) at pH 3, where we observed that the presence of Cu^{2+} ions is unable to quench the fluorescence intensity of NANO-PAMAM-CHT, but the presence of $Cr_2O_7^{2-}$ is selectively able to quench the fluorescence intensity efficiently. Mechanistic study reveals dynamic quenching of NANO-PAMAM-CHT in the presence of Cu^{2+} ions and static quenching in the presence of $Cr_2O_7^{2-}$ ions. Additionally, time dependent study exhibits a fast response time and a temperature dependent study affirms that the microgel can be used in a wide range of ambient temperatures (25 °C–45 °C), without any impact on its performance.

Results and discussion

Synthesis and characterization

NANO-PAMAM-CHT microgels are prepared *via* aza-Michael reaction in water, as illustrated in Scheme 1. Initially, as per the established reported protocol by our group,[48] NANO-PAMAM is synthesized in a two-step process. The first step

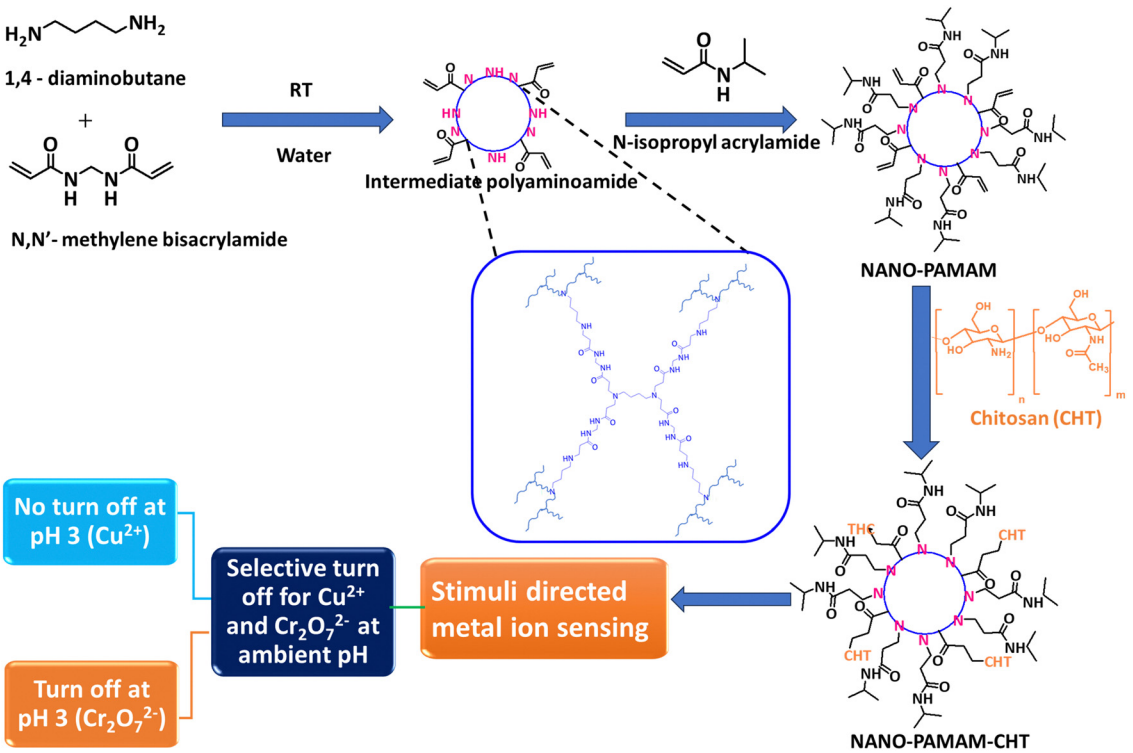

Scheme 1 Synthetic scheme for the NANO-PAMAM-CHT microgels and its application towards the selective detection of Cu^{2+} and $Cr_2O_7^{2-}$ in water.

 This journal is © The Royal Society of Chemistry 2024

Published on 13 November 2023. Downloaded on 07/09/2025 11:09:43 PM.

involves the preparation of intermediate poly(aminoamide) *via* reaction between 1,4-diaminobutane and *N*,*N*-methylene-bisacrylamide, and the second step involves the functionalization of *N*-isopropylacrylamide to prepare the stable NANO-PAMAM nanogel. In the next stage, the aza-Michael addition reaction between acryl-amide functional groups of NANO-PAMAM and free amine groups of chitosan in water at room temperature leads to the formation of NANO-PAMAM-CHT.

The reaction conditions were screened with different weight ratios of NANO-PAMAM and chitosan, to optimise the formation of NANO-PAMAM-CHT microgels (Fig. S1, ESI†). To analyse the reaction, the disappearance of the prominent peaks for acryl amide protons of NANO-PAMAM at around 5.5–6.5 ppm was monitored by varying the weight ratio of NANO-PAMAM to chitosan (1 : 1, 1 : 1.5 and 1 : 2) in the presence of base, DABCO (Table S1, ESI†). At the weight ratio of NANO-PAMAM to chitosan (1 : 2), we can achieve 100% conversion to the product (NANO-PAMAM-CHT) in the presence of DABCO (as a base). The NANO-PAMAM-CHT microgel was purified *via* precipitation in acetone and characterized by different techniques. ^{1}H NMR spectra analysis (Fig. 1A) reveals the presence of characteristic peaks of both chitosan and poly(aminoamide) backbone as assigned, with a complete disappearance of (CH_2═CH–) proton peaks of acrylamides (which are present in NANO-PAMAM). This reveals the formation of NANO-PAMAM-CHT *via* aza-Michael addition reaction.

Furthermore, the formation of the NANO-PAMAM-CHT microgels was affirmed by FTIR spectra (Fig. 1B). In the case of chitosan (CHT), the typical stretching band of the –OH group and –NH_2 group appeared at 3400–3322 cm^{-1}. The stretching band of amino (N–H) bending corresponds to the peaks at 1650 cm^{-1} and 1583 cm^{-1}. For primary alcohol (C–OH) and methylene (CH_2) groups, stretching bands are coming at 1022 cm^{-1} and 1367 cm^{-1} respectively. For NANO-PAMAM-CHT (NANO-PAMAM modified with the free amine group of chitosan), a C═O stretching band appeared at 1642 cm^{-1} and the disappearance of the IR bands at 2962 cm^{-1} is for (C═C–H). This supports the successful synthesis of NANO-PAMAM-CHT *via* the aza-Michael addition reaction between the acrylamide group of NANO-PAMAM and the free amine group of chitosan.

Thermogravimetric analysis (TGA) of the NANO-PAMAM-CHT was done from room temperature to 800 °C to reveal the thermal stability and structure (Fig. S2, ESI†). From the TGA thermogram, initially ∼10% weight loss was observed around 100 °C, which can be attributed to the moisture present, due to the hygroscopic nature of the microgel backbone. In the second step, the weight loss at around 200 °C, can be primarily attributed to the thermal degradation of the chitosan backbone[49] and in the final stage, weight loss at around 280 °C is attributed to the degradation of the poly(aminoamide) backbone of NANO-PAMAM-CHT, in addition to the ongoing chitosan backbone.[50–52]

Size exclusion chromatography (SEC), was used to analyze the average molecular weight of NANO-PAMAM-CHT (Fig. S3, ESI†). The average molecular weight of the microgel was in the order of 10^5 Da.

To understand the size and morphology, the microgels were analyzed using DLS, AFM and TEM. For a better understanding, NANO-PAMAM and NANO-PAMAM-CHT are compared through

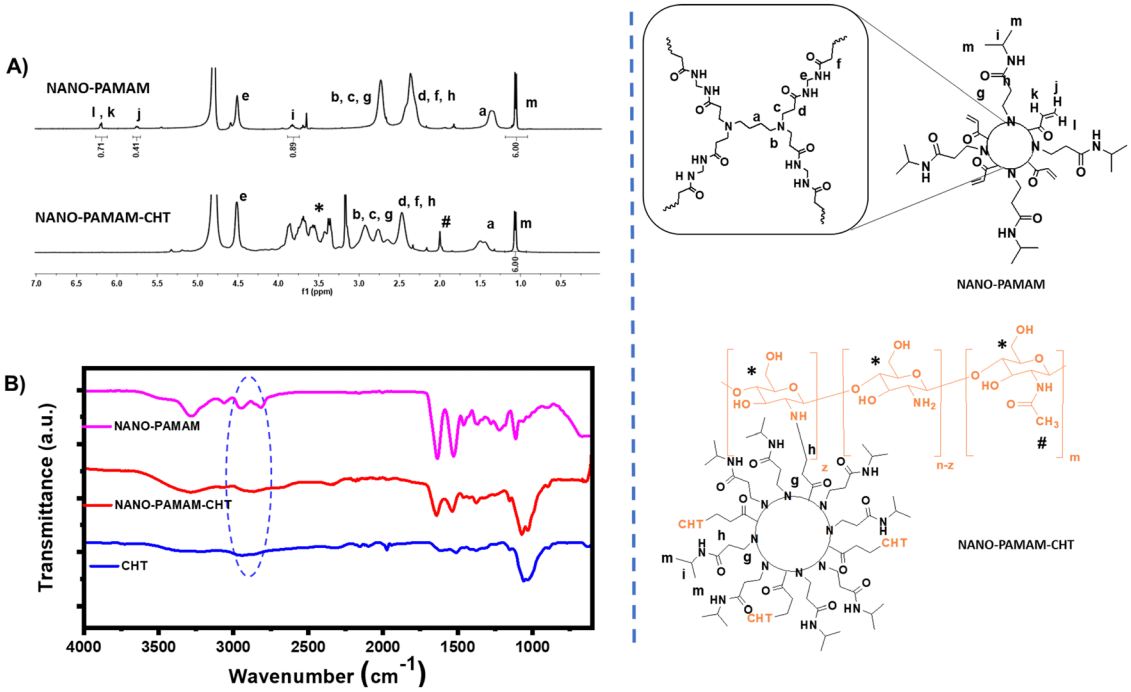

Fig. 1 (A) ^{1}H-NMR analysis of NANO-PAMAM and NANO-PAMAM-CHT (NANO-PAMAM: CHT = 1 : 2, wt. ratio). (B) FT-IR spectra analysis of NANO-PAMAM, NANO-PAMAM-CHT and chitosan (CHT).

Published on 13 November 2023. Downloaded on 07/09/2025 11:09:43 PM.

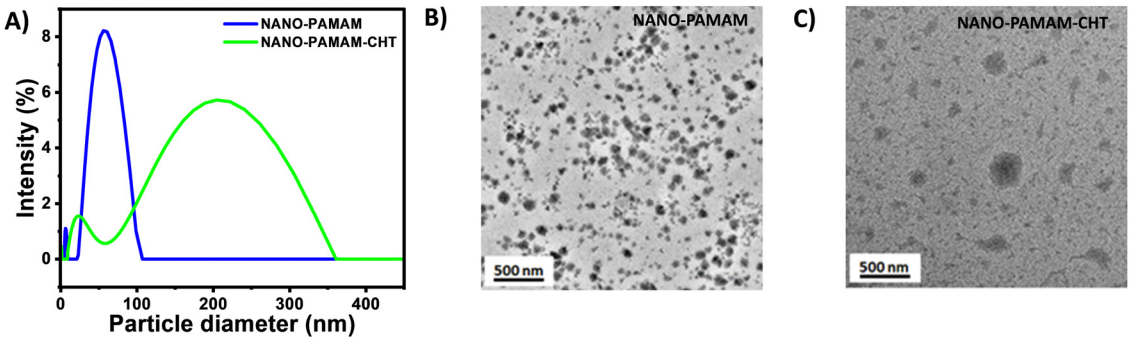

Fig. 2 (A) DLS of NANO-PAMAM and NANO-PAMAM-CHT. (B) TEM micrograph of NANO-PAMAM and (C) TEM micrograph of NANO-PAMAM-CHT (after reacting with chitosan).

all the analyses. The average hydrodynamic diameter of the NANO-PAMAM increases from ∼60 nm to ∼200 nm (Fig. 2A) after modification with chitosan (NANO-PAMAM-CHT). Fig. 2B exhibits the transmission electron microgram of NANO-PAMAM, where we have seen that the size of the NANO-PAMAM lies in the range of around 40 nm to 60 nm. Whereas, in Fig. 2C, we observed that the size of NANO-PAMAM-CHT increases to 150 nm to 250 nm. Additionally, the AFM analysis of NANO-PAMAM-CHT revealed the presence of irregular microstructures that were also evident from the 3D structure of NANO-PAMAM-CHT as shown in Fig. S4B (ESI†) and the diameter of NANO-PAMAM-CHT lies in the range of 150–200 nm (Fig. S4A, ESI†). From the height profile graph of NANO-PAMAM-CHT, we can conclude that the microgel was flattened and spread over the substrate surface due to its soft nature (Fig. S4A, ESI†).

pH responsive optical properties of the NANO-PAMAM-CHT

NANO-PAMAM-CHT was excited at 370 nm to analyse the blue emission property (as observed under UV light) where the spectra reveal λ_{max} = 440 nm (Fig. 3A). The fluorescence property of NANO-PAMAM-CHT is attributed largely to the nonconventional fluorescent polyaminoamide core (NANO-PAMAM). Compared with the NANO-PAMAM, the λ_{max} of the NANO-PAMAM-CHT microgel is slightly red-shifted (∼27 nm) and a hyper-chromic shift was noted (likely the effect of chitosan). The CIE 1931 color coordinate diagram confirms the blue emission of NANO-PAMAM-CHT, where the (*X*, *Y*) coordinates are (0.16, 0.14), as shown in Fig. S5, ESI.†

To further understand the influence of pH, the emission spectra of NANO-PAMAM-CHT were studied in a range of pHs by using a spectrofluorometer (Fig. S6, ESI†). Fig. 3B exhibits the variation of fluorescence intensity with changing the pH – a significant increment in fluorescence intensity was noted as the pH of the solution rises from pH 3 to pH 11. A probable hypothesis behind this is that, at the higher/basic pH, amine groups are deprotonated, which results in an increase in the formation of localized clusters due to more favourable intra-molecular interactions, resulting in an increase in fluorescence intensity.[53]

Sensing of different metal ions

A fluorescence screening experiment was performed at ambient pH (pH ∼7) to observe the selectivity of the synthesized NANO-PAMAM-CHT microgel toward different ions. Two sets of experiments were performed for the screening of both cations and anions. Fig. 4A exhibits the emission spectra of photo-luminescence activity for NANO-PAMAM-CHT with the addition of Cu^{2+}, Zn^{2+}, Ca^{2+}, Mn^{2+}, Fe^{2+}, Fe^{3+}, Cr^{3+}, Ba^{2+}, Mg^{2+}, Ni^{2+}, Co^{2+}, Pb^{2+}, Cd^{2+}, Na^{+}, and K^{+} metal ion solutions (10 mM). The

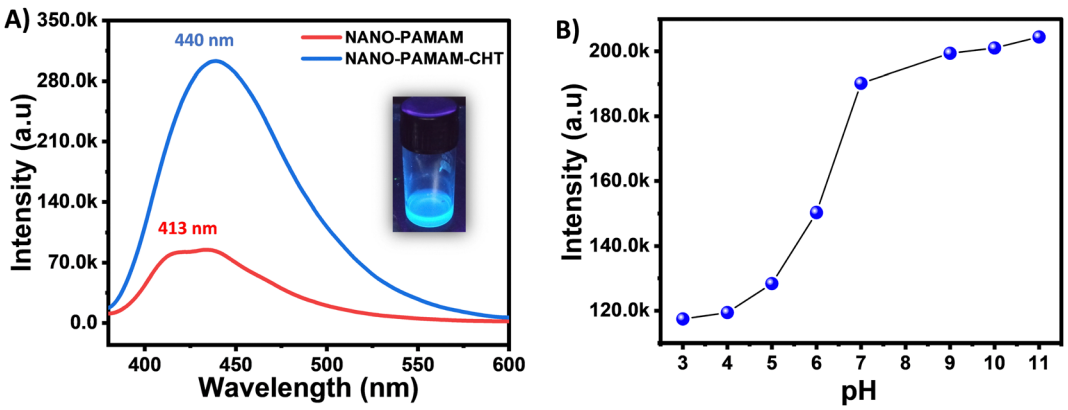

Fig. 3 (A) Fluorescence emission spectra of NANO-PAMAM and NANO-PAMAM-CHT (inset: the picture of NANO-PAMAM-CHT solution under UV light). (B) Variation of the fluorescence intensity as a function of different pH.

 This journal is © The Royal Society of Chemistry 2024

Published on 13 November 2023. Downloaded on 07/09/2025 11:09:43 PM.

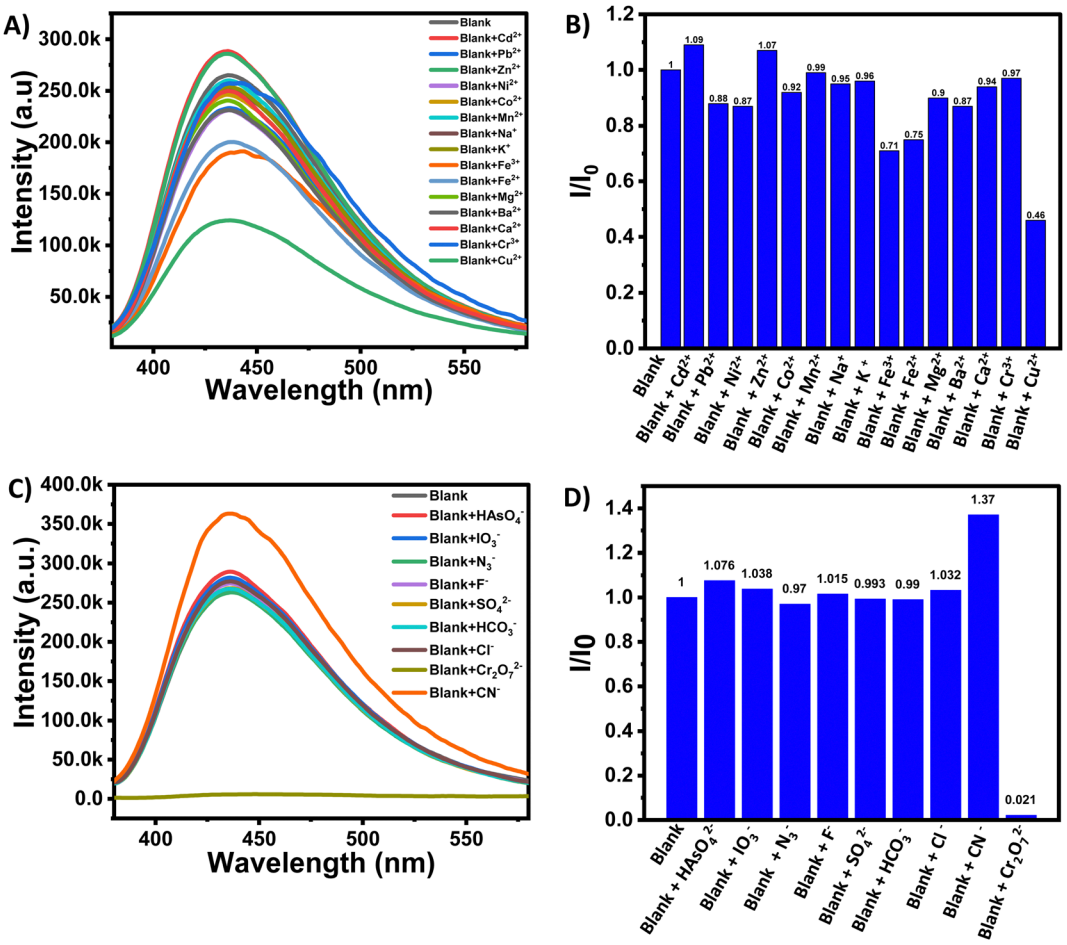

Fig. 4 (A) Fluorescence emission spectra of NANO-PAMAM-CHT in the presence of different metal ions with excitation at 370 nm. (B) Selectivity of NANO-PAMAM-CHT towards Cu^{2+} ions. (C) Fluorescence emission spectra of NANO-PAMAM-CHT in the presence of different anions with excitation at 370 nm. (D) Selectivity of NANO-PAMAM-CHT towards $Cr_2O_7^{2-}$ ions.

selectivity was measured by plotting I/I_0 (intensity ratio) with the same concentration of different metal ion solutions, where I and I_0 indicate the photoluminescence intensity of the microgel solution (with excitation at 370 nm) in the presence of different metal ions and in the absence of any metal ions, respectively. The obtained histogram (Fig. 4B) reveals that in the presence of Cu^{2+}, the I/I_0 ratio significantly decreased compared to the other metal ions. This signifies that the NANO-PAMAM-CHT exhibits selective turn off behaviour in the presence of Cu^{2+} solutions. With interference from other metal ions, the sensing and selectivity are vulnerable in the chemical detector. Using various metal ions, we performed competitive experiments (Fig. S7, ESI†) to authenticate the selectivity of NANO-PAMAM-CHT towards Cu^{2+} ions. The fluorescence intensities of NANO-PAMAM-CHT were not reduced significantly in the presence of various metal ions but the fluorescence intensities decreased significantly on further addition of Cu^{2+} ions (Fig. S8, ESI†). Hence, this result infers that without interference from other metal ions, NANO-PAMAM-CHT selectively detects Cu^{2+} ions. From these results, we can conclude that NANO-PAMAM-CHT ensured recognizable advantages in detecting copper ions.

Similarly, to study the selectivity for different anions, the emission spectra of NANO-PAMAM-CHT were measured in the presence of different anions, using NaX solution, where X = $HAsO_4^{2-}$, IO_3^-, N_3^-, F^-, SO_4^{2-}, HCO_3^-, Cl^-, CN^- and $Cr_2O_7^{2-}$. From the fluorescence spectra analysis (Fig. 4C), we observed that the fluorescence intensity of NANO-PAMAM-CHT in the presence of $HAsO_4^{2-}$, IO_3^-, N_3^-, F^-, SO_4^{2-}, HCO_3^-, Cl^-, and CN^- did not change significantly but the same is selectively decreased in the presence of $Cr_2O_7^{2-}$. Similar analysis of I/I_0 (intensity ratio) with the same concentration of different anionic analytes reveals significant and selective turn off for $Cr_2O_7^{2-}$ (Fig. 4D). This indicates that NANO-PAMAM-CHT microgels can act as a probe for the selective detection of $Cr_2O_7^{2-}$ ions.

To understand the interference of other anions on NANO-PAMAM-CHT, we carried out a competitive experiment in the presence of $Cr_2O_7^{2-}$ ions with other anions like $HAsO_4^{2-}$, IO_3^-, N_3^-, F^-, SO_4^{2-}, CN^-, HCO_3^- and Cl^- (Fig. S9, ESI†). The incorporation of equivalent molar interfering anions $HAsO_4^{2-}$, IO_3^-, N_3^-, F^-, SO_4^{2-}, CN^-, HCO_3^- and Cl^- into the aqueous solution of NANO-PAMAM-CHT at pH 7 did not affect its

Published on 13 November 2023. Downloaded on 07/09/2025 11:09:43 PM.

fluorescence intensity but the fluorescence intensities decreased significantly on further addition of $Cr_2O_7^{2-}$ ions (Fig. S10, ESI†). Hence, this result concludes that without interference from other anions, NANO-PAMAM-CHT selectively detects $Cr_2O_7^{2-}$ ions.

The Stern–Volmer equation was used for the analysis of the quenching effect quantitatively for both Cu^{2+} ions and $Cr_2O_7^{2-}$ ions and the equation is expressed as:

$$I_0/I = 1 + K_{SV}[Q]$$

where I_0 is the fluorescence intensity before the addition of analytes and I is the fluorescence intensity after the addition of analytes, K_{SV} is known as the Stern–Volmer constant, and $[Q]$ is the analyte concentration. In the range from 0–25 μM, a consistent decrease in fluorescence intensity was observed with increasing concentration of Cu^{2+} ions (Fig. 5A). A good linear relationship was observed by plotting the relative intensity (I_0/I) against increasing concentration of copper solution, where the value of correlation coefficient (R^2) was 0.999 and K_{SV} = 2722.24 M^{-1}, as presented in Fig. 5B. The calculated limit of detection (LOD) was 16.9 μM (Fig. S11, ESI†) using the equation LOD = $3\delta/k$, where δ is standard deviation and k is the slope obtained from the intensity *vs.* concentration plot. It is important to note that the LOD is lower compared to the allowed limit of Cu^{2+} in drinking water as approved by the US Environmental Protection Agency (EPA).[42]

Similarly for dichromate anion, the fluorescence intensity of NANO-PAMAM-CHT was studied within the analyte concentration range of 0.00–36 μM (Fig. 5C), and a linear correlation coefficient (R^2) of 0.996 and a K_{SV} value of 22 180 M^{-1} was reported as calculated using the Stern–Volmer equation (Fig. 5D). From the fluorescence emission intensity of NANO-PAMAM-CHT, the high K_{sv} value indicates the relatively high quenching efficiency for $Cr_2O_7^{2-}$.

The limit of detection (LOD) of $Cr_2O_7^{2-}$ was calculated as 2.62 μM (Fig. S12, ESI†). Herein, it is important to note that the LOD is lower compared to the allowed level of dichromate contamination in drinking water according to the American Water Works Association: Denver, CO, USA (5 μM).[46] A comparison was studied for NANO-PAMAM-CHT with the other sensors in the presence of Cu^{2+} and $Cr_2O_7^{2-}$ and tabulated in Tables S2 and S3 (ESI†), respectively. A time-dependent quenching study was done in the presence of Cu^{2+} ions and $Cr_2O_7^{2-}$ ions, respectively (Fig. S13 and S14, ESI†). Fig. S15 (ESI†) reveals that NANO-PAMAM-CHT can detect both analytes within a minute,

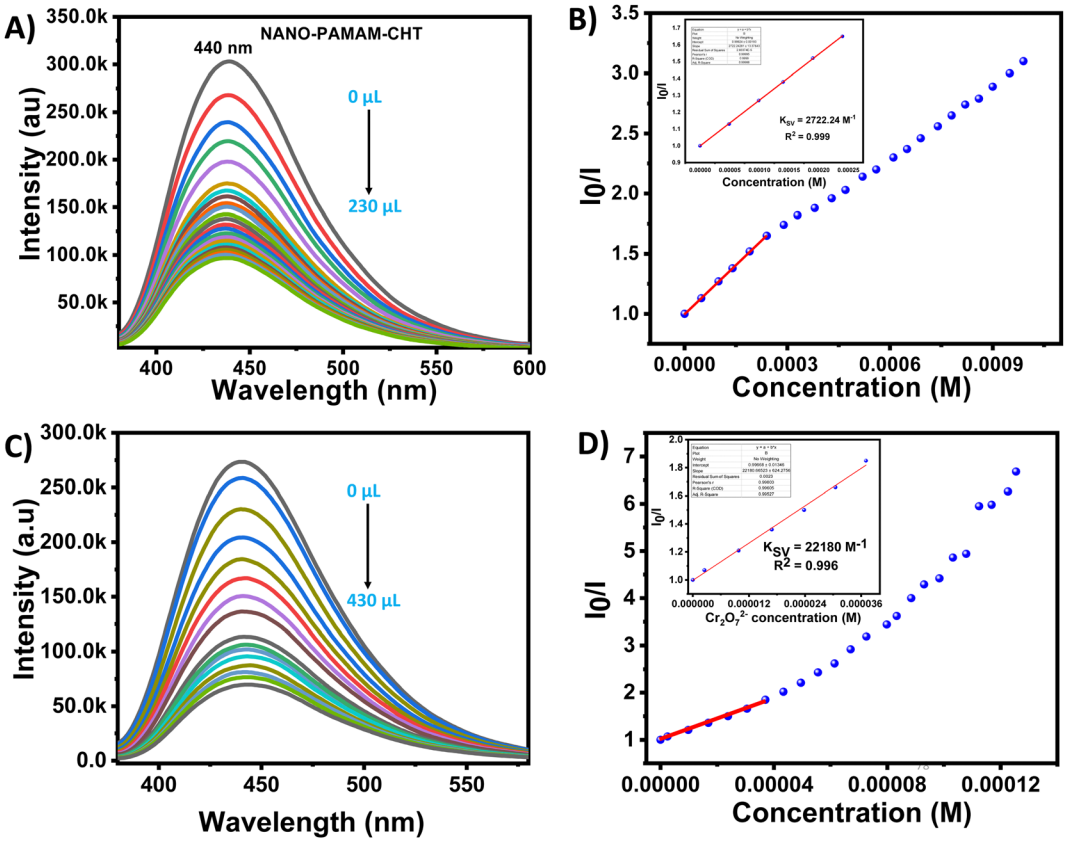

Fig. 5 (A) Quenching of the fluorescence intensity of NANO-PAMAM-CHT by aqueous solution of Cu^{2+} ions under excitation at 370 nm with slit 2. (B) Stern–Volmer plot for NANO-PAMAM-CHT by Cu^{2+} solution; the inset picture shows the K_{sv} plot at the lower concentration region in the presence of Cu^{2+} ions. (C) Quenching of the fluorescence intensity of NANO-PAMAM-CHT by an aqueous solution of $Cr_2O_7^{2-}$ ions under excitation at 370 nm with slit 2. (D) Stern–Volmer plot for NANO-PAMAM-CHT by $Cr_2O_7^{2-}$ solution; the inset picture shows the K_{sv} plot at the lower concentration region in the presence of $Cr_2O_7^{2-}$ions.

 This journal is © The Royal Society of Chemistry 2024

Published on 13 November 2023. Downloaded on 07/09/2025 11:09:43 PM.

signifying fast response time for the demonstrated detections. Additionally, we have studied the temperature-dependent fluorescence behaviour of NANO-PAMAM-CHT at 25 °C and at 45 °C in the presence of both Cu^{2+} ions and $Cr_2O_7^{2-}$ ions (Fig. S16–S19, ESI†). It was noted that the fluorescence intensity ratio (I_0/I) of NANO-PAMAM-CHT was not affected by increasing temperature; this reveals that the microgels are useful in various temperature and climate regions, without changing their efficiency.

pH-dependent discrimination of Cu^{2+} and $Cr_2O_7^{2-}$

As both Cu^{2+} and $Cr_2O_7^{2-}$ were detected by a turn off mechanism, it is further important to differentiate between them for highly specific sensing. For that purpose, a pH responsive study was conducted for both the analytes at lower pH (acidic, pH ∼3). NANO-PAMAM-CHT consists of hyper-branched polyaminoamide and chitosan moieties, and contains protonable $-NH_2$ groups. It is expected that due to higher protonation of amine with the NANO-PAMAM-CHT, interactions with Cu^{2+} will be restricted at lower pH. From Fig. 6A and B, it was observed that the original fluorescence intensity of NANO-PAMAM-CHT was not significantly reduced at pH 3 in the presence of Cu^{2+} ions. On the other hand, the presence of $Cr_2O_7^{2-}$ ions significantly quenched the fluorescence intensity of NANO-PAMAM-CHT. A plot summarizing the concentration dependent study within the range between 0–690 μM clearly revealed a clear decrease in fluorescence intensity in the presence of $Cr_2O_7^{2-}$ (Fig. 6D), whereas absolutely no change in the presence of Cu^{2+} ions was noted (Fig. 6C). This confirms that NANO-PAMAM-CHT can selectively detect $Cr_2O_7^{2-}$, in the presence of Cu^{2+} at pH ∼3. From the plot, a

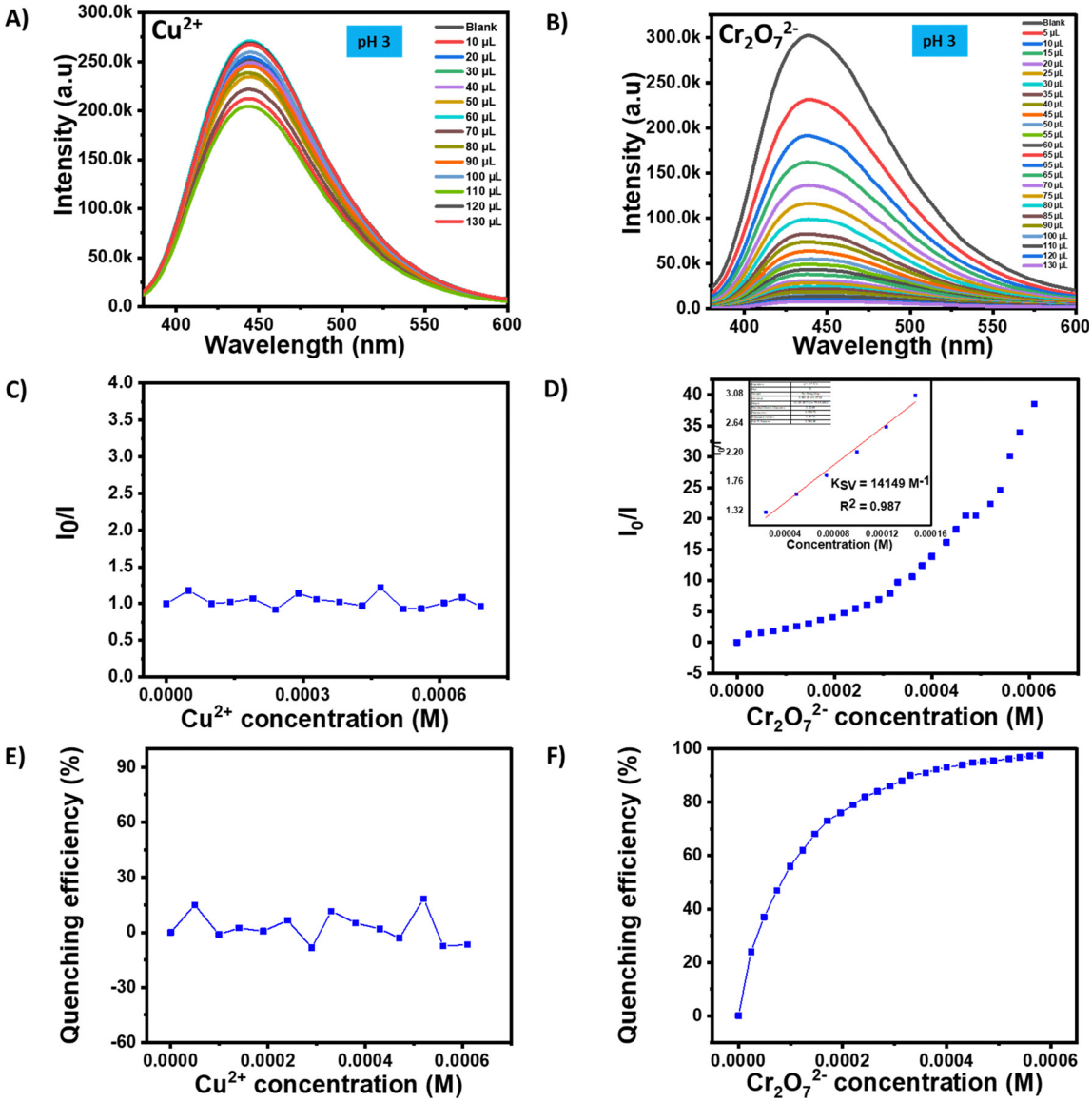

Fig. 6 (A) and (B) Fluorescence emission spectra of NANO-PAMAM-CHT in the presence of Cu^{2+} and $Cr_2O_7^{2-}$ at pH 3. (C) and (D) K_{sv} plot of NANO-PAMAM-CHT with the addition of Cu^{2+} and $Cr_2O_7^{2-}$ at pH 3. (E) and (F) Quenching efficiency plot of NANO-PAMAM-CHT with the addition of Cu^{2+} and $Cr_2O_7^{2-}$ at pH 3.

Published on 13 November 2023. Downloaded on 07/09/2025 11:09:43 PM.

correlation coefficient (R^2) = 0.987 and K_{SV} = 14 149 M^{-1} (inset picture of Fig. 6D) was reported for $Cr_2O_7^{2-}$ at pH ~3. The calculated limit of detection (LOD) for $Cr_2O_7^{2-}$ at pH ~3 was 8.08 μM (Fig. S20, ESI†). Further studies were continued to understand the performance of NANO-PAMAM-CHT towards sensing of both Cu^{2+} and $Cr_2O_7^{2-}$ under basic pH (pH ~9). It was noted that the microgel can sense both the analytes without any discrimination (unlike pH ~3). The limit of detection (LOD) of both $Cr_2O_7^{2-}$ (Fig. S21, ESI†) and Cu^{2+} (Fig. S22, ESI†) was calculated as 3.1 μM and 31 μM respectively at pH ~9.

Mechanism of sensing

Fluorescence quenching can occur mainly due to three reasons, (i) fluorescent materials transferred into non-fluorescent materials, (ii) electron transfer, and (iii) the inner filter effect.[54] For the quenching incident, different mechanisms are generally known, such as dynamic quenching, static quenching, and competitive absorption. Static quenching may happen due to the formation of the ground state complex/interactions. On the other hand, dynamic quenching involves the process of collision in the excited state. To get more information about the dynamic and static mechanisms, the time-correlated single photon counting (TCSPC) technique was carried out.[30] A clear decrease in the average lifetime (obtained using the decay parameter in Table S4, ESI†) of the NANO-PAMAM-CHT was identified from 5.48 ns to 4.89 ns in the absence and presence of Cu^{2+} ions in the aqueous solution of NANO-PAMAM-CHT, which supported the dynamic quenching process in the presence of Cu^{2+} ions (Fig. 7A). After the addition of $Cr_2O_7^{2-}$ solution into the aqueous solution of NANO-PAMAM-CHT, no such noticeable variation of average lifetime (using decay parameters in Table S5, ESI†) was observed. Hence, a static quenching process may be involved in the quenching phenomenon of NANO-PAMAM-CHT in the presence of $Cr_2O_7^{2-}$ ions (Fig. 7B). To further affirm this, UV-vis spectra of aqueous solutions of NANO-PAMAM-CHT (Fig. 7C) in the presence of dichromate ion were recorded. The absorption peak originating at around 370 nm supported the ground state interaction between NANO-PAMAM-CHT and $Cr_2O_7^{2-}$ ions (Fig. 7C). Besides, compared with pure dichromate solution, the absorption peak was significantly red shifted (20 nm) compared to the absorption peak of pure dichromate (Fig. S23, ESI†). Hence, combination of both the studies supported the static quenching phenomenon of NANO-PAMAM-CHT in the presence of $Cr_2O_7^{2-}$ ions.[55] On the other hand, with the addition of Cu^{2+} ions, we did not observe such a shift of the absorption peak.

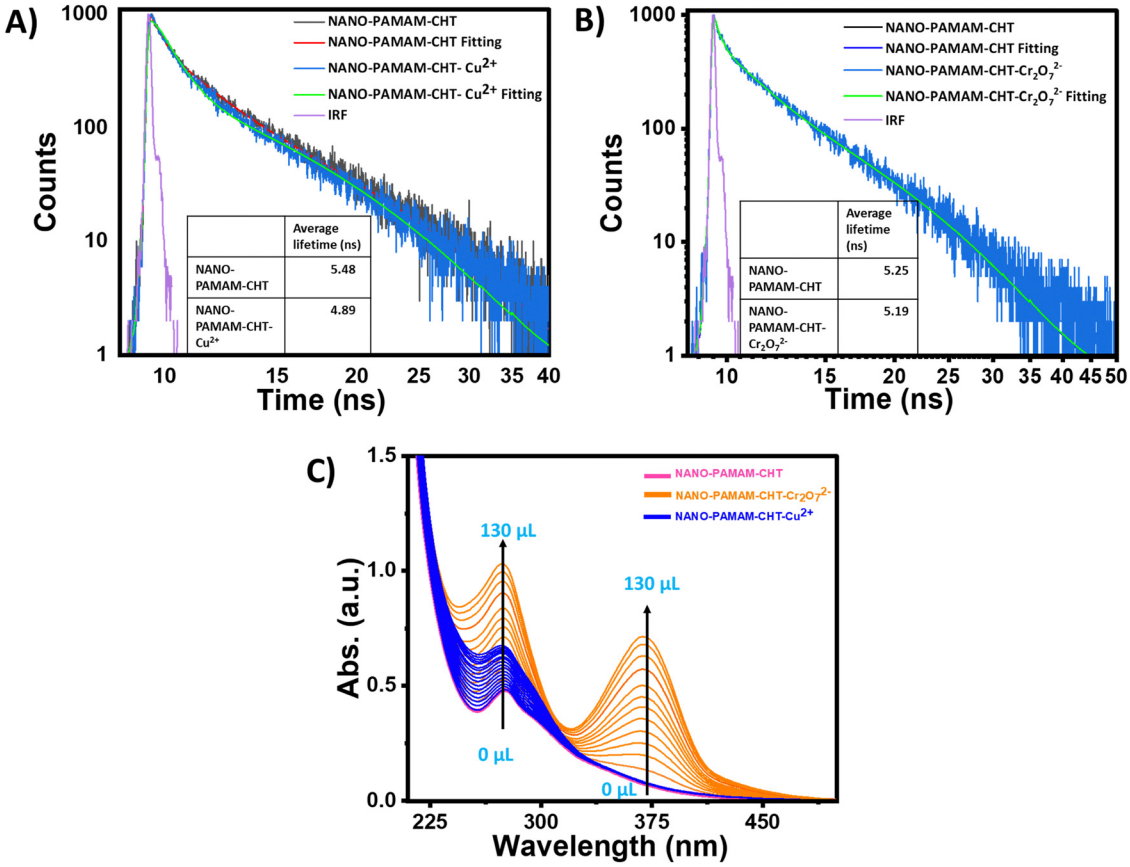

Fig. 7 (A) Fluorescence decay with excitation at 375 nm for NANO-PAMAM-CHT in the absence and presence of Cu^{2+} ions by using the time-correlated single photon counting (TCSPC) technique. (B) Fluorescence decay with excitation at 375 nm for NANO-PAMAM-CHT in the absence and presence of $Cr_2O_7^{2-}$ ions by using the time-correlated single photon counting (TCSPC) technique. (C) UV-vis absorption spectra of NANO-PAMAM-CHT with the addition of $Cr_2O_7^{2-}$ and Cu^{2+} ions.

 This journal is © The Royal Society of Chemistry 2024

Published on 13 November 2023. Downloaded on 07/09/2025 11:09:43 PM.

Conclusion

In summary, the synthesis of a water-soluble pH responsive fluorescent microgel (NANO-PAMAM-CHT) is reported *via* aza-Michael addition reaction between an acrylamide functional aminoamide (NANO-PAMAM) and chitosan in water at room temperature. The reaction was monitored *via* NMR spectroscopy and the final microgel was further characterized by IR, SEC, TGA, DLS, TEM and AFM. This microgel can show a pH responsive fluorescent property from pH 3 to pH 11. A detailed study reveals that the microgel can selectively detect Cu^{2+} and $Cr_2O_7^{2-}$ ions in water under ambient pH within a minute and their calculated limits of detection are 16.9 μM and 2.62 μM, respectively (both are below than minimum allowed level). Moreover, it can selectively differentiate between Cu^{2+} and $Cr_2O_7^{2-}$ at pH $\sim$3, where selective quenching is only noted for $Cr_2O_7^{2-}$ in aqueous media. The mechanistic study supported by the fluorescence decay and the UV-vis spectra analysis, further supported the existence of a dynamic quenching phenomenon in the presence of Cu^{2+} and static quenching in the presence of $Cr_2O_7^{2}$. Moreover, time and temperature-dependent studies revealed a fast response time (within a minute) and its efficient usefulness in a wide range of temperatures.

Author contributions

S. G. performed all the experiments and analysis. J. D. K. performed the reaction between NANO-PAMAM and chitosan. S. C. supervised the work and received the funding.

Conflicts of interest

There are no conflicts to declare.

Acknowledgements

S. G. and J. D. K. acknowledge IITP for the research fellowship and SC acknowledges CSIR (02(0370)/19/EMRII) for funding the work.

Notes and references

1 M. R. Awual, I. M. M. Rahman, T. Yaita, M. A. Khaleque and M. Ferdows, *Chem. Eng. J.*, 2014, **236**, 100–109.
2 Z. Ö. Kocabaş-Ataklı and Y. Yürüm, *Chem. Eng. J.*, 2013, **225**, 625–635.
3 A. H. Sulaymon, B. A. Abid and J. A. Al-Najar, *Chem. Eng. J.*, 2009, **155**, 647–653.
4 N. Choudhury, B. Saha and P. De, *Eur. Polym. J.*, 2021, **145**, 110233.
5 V. Kumar, S. K. Saini, N. Choudhury, A. Kumar, B. Maiti, P. De, M. Kumar and S. Satapathi, *ACS Appl. Polym. Mater.*, 2021, **3**, 4017–4026.
6 K. P. Carter, A. M. Young and A. E. Palmer, *Chem. Rev.*, 2014, **114**, 4564–4601.
7 N. Choudhury, B. Ruidas, C. D. Mukhopadhyay and P. De, *ACS Appl. Polym. Mater.*, 2020, **2**, 5077–5085.
8 X. Chen, M. J. Jou, H. Lee, S. Kou, J. Lim, S.-W. Nam, S. Park, K.-M. Kim and J. Yoon, *Sens. Actuators, B*, 2009, **137**, 597–602.
9 S. Erdemir, B. Tabakci and M. Tabakci, *Sens. Actuators, B*, 2016, **228**, 109–116.
10 Z.-H. Liu, S. Devaraj, C.-R. Yang and Y.-P. Yen, *Sens. Actuators, B*, 2012, **174**, 555–562.
11 Q. Wu, X. Wang, S. A. Rasaki, T. Thomas, C. Wang, C. Zhang and M. Yang, *J. Mater. Chem. C*, 2018, **6**, 4508–4515.
12 N. Gogoi, M. Barooah, G. Majumdar and D. Chowdhury, *ACS Appl. Mater. Interfaces*, 2015, **7**, 3058–3067.
13 A. Jaiswal, S. S. Ghsoh and A. Chattopadhyay, *Langmuir*, 2012, **28**, 15687–15696.
14 T. Boobalan, M. Sethupathi, N. Sengottuvelan, P. Kumar, P. Balaji, B. Gulyás, P. Padmanabhan, S. T. Selvan and A. Arun, *ACS Appl. Nano Mater.*, 2020, **3**, 5910–5919.
15 H. Barhum, T. Alon, M. Attrash, A. Machnev, I. Shishkin and P. Ginzburg, *ACS Appl. Nano Mater.*, 2021, **4**, 9919–9931.
16 M. M. R. Khan, T. Mitra and D. Sahoo, *RSC Adv.*, 2020, **10**, 9512–9524.
17 X. Gao, C. Du, Z. Zhuang and W. Chen, *J. Mater. Chem. C*, 2016, **4**, 6927–6945.
18 H. Bai, Z. Tu, Y. Liu, Q. Tai, Z. Guo and S. Liu, *J. Hazard. Mater.*, 2020, **386**, 121654.
19 G. K. Darbha, A. K. Singh, U. S. Rai, E. Yu, H. Yu and P. Chandra Ray, *J. Am. Chem. Soc.*, 2008, **130**, 8038–8043.
20 P. Daga, P. Majee, D. K. Singha, P. Manna, S. Hui, A. K. Ghosh, P. Mahata and S. K. Mondal, *New J. Chem.*, 2020, **44**, 4376–4385.
21 N. Choudhury, B. Ruidas, B. Saha, K. Srikanth, C. D. Mukhopadhyay and P. De, *Polym. Chem.*, 2020, **11**, 2015–2026.
22 N. Choudhury, S. Mete, S. Kambalapalli and P. De, *J. Polym. Sci., Part A: Polym. Chem.*, 2018, **56**, 914–921.
23 S. Xiong, L. Duan and X. Cheng, *Polym. Chem.*, 2020, **11**, 6066–6072.
24 P. M. Reddy, S.-R. Hsieh, W.-C. Wu, C.-J. Chang, Y.-S. Chen and M.-C. Lee, *React. Funct. Polym.*, 2018, **123**, 26–33.
25 S. Xiong, W. Sun, R. Chen, Z. Yuan and X. Cheng, *Carbohydr. Polym.*, 2021, **273**, 118590.
26 G. Pina-Luis, M. Martínez-Quiroz, A. Ochoa-Terán, H. Santacruz-Ortega and E. Mendez-Valenzuela, *J. Lumin.*, 2013, **134**, 729–738.
27 P. M. Reddy, S.-R. Hsieh, M.-C. Lee, C.-J. Chang, A. Pundi, Y.-S. Chen, C.-H. Lu and J.-M. Yeh, *Dyes Pigm.*, 2019, **164**, 327–334.
28 D. Zhang, Y. Qi, Y. Li, Y. Song, C. Xian, H. Li and P. Cong, *J. Fluoresc.*, 2021, **31**, 1133–1141.
29 N. Kumari, N. Dey, S. Jha and S. Bhattacharya, *ACS Appl. Mater. Interfaces*, 2013, **5**, 2438–2445.
30 S. Dong, W. Ji, Z. Ma, Z. Zhu, N. Ding, J. Nie and B. Du, *ACS Appl. Polym. Mater.*, 2020, **2**, 3621–3631.
31 S. Kumari, M. Avais and S. Chattopadhyay, *ACS Appl. Polym. Mater.*, 2023, **5**, 1626–1645.

Published on 13 November 2023. Downloaded on 07/09/2025 11:09:43 PM.

32 Q. Miao, Z. Wu, Z. Hai, C. Tao, Q. Yuan, Y. Gong, Y. Guan, J. Jiang and G. Liang, *Nanoscale*, 2015, **7**, 2797–2804.
33 M. Dong, Y.-W. Wang and Y. Peng, *Org. Lett.*, 2010, **12**, 5310–5313.
34 Z.-Q. Hu, C.-s Lin, X.-M. Wang, L. Ding, C.-L. Cui, S.-F. Liu and H. Y. Lu, *Chem. Commun.*, 2010, **46**, 3765–3767.
35 L. Xu, Y. Xu, W. Zhu, B. Zeng, C. Yang, B. Wu and X. Qian, *Org. Biomol. Chem.*, 2011, **9**, 8284–8287.
36 P. Majee, D. K. Singha, S. K. Mondal and P. Mahata, *Photochem. Photobiol. Sci.*, 2019, **18**, 1110–1121.
37 J. Kaushik, D. Saini, R. Singh, P. Dubey and S. K. Sonkar, *New J. Chem.*, 2021, **45**, 20164–20172.
38 L. Li, S. Shen, R. Lin, Y. Bai and H. Liu, *Chem. Commun.*, 2017, **53**, 9986–9989.
39 Y.-Z. Chen and H.-L. Jiang, *Chem. Mater.*, 2016, **28**, 6698–6704.
40 B. Wen, J. Xue, X. Zhou, Q. Wu, J. Nie, J. Xu and B. Du, *ACS Appl. Mater. Interfaces*, 2018, **10**, 25706–25716.
41 J. Yin, X. Guan, D. Wang and S. Liu, *Langmuir*, 2009, **25**, 11367–11374.
42 L. M. Gaetke, H. S. Chow-Johnson and C. K. Chow, *Arch. Toxicol.*, 2014, **88**, 1929–1938.
43 C. Zong, K. Ai, G. Zhang, H. Li and L. Lu, *Anal. Chem.*, 2011, **83**, 3126–3132.
44 Z.-J. Lin, H.-Q. Zheng, H.-Y. Zheng, L.-P. Lin, Q. Xin and R. Cao, *Inorg. Chem.*, 2017, **56**, 14178–14188.
45 S. Mohandoss, J. Sivakamavalli, B. Vaseeharan and T. Stalin, *Sens. Actuators, B*, 2016, **234**, 300–315.
46 A. W. W. Association, *J. Am. WATER Work. Assoc.*, 2013.
47 S. Lv, S. Liang, J. Zuo and S. Zhang, *Analyst*, 2022, **147**, 4657–4673.
48 S. Ghosh, M. Avais and S. Chattopadhyay, *Chem. Commun.*, 2022, **58**, 12807–12810.
49 J. D. Katiyar and S. Chattopadhyay, *Carbohydr. Polym.*, 2022, **287**, 119324.
50 M. Avais and S. Chattopadhyay, *ACS Appl. Polym. Mater.*, 2021, **3**, 789–800.
51 M. Avais and S. Chattopadhyay, *J. Mater. Chem. A*, 2022, **10**, 20090–20100.
52 M. Avais, S. Kumari and S. Chattopadhyay, *Soft Matter*, 2021, **17**, 6383–6393.
53 R.-b Wang, W.-z Yuan and X.-y Zhu, *Chin. J. Polym. Sci.*, 2015, **33**, 680–687.
54 L. Lin, M. Rong, S. Lu, X. Song, Y. Zhong, J. Yan, Y. Wang and X. Chen, *Nanoscale*, 2015, **7**, 1872–1878.
55 A. S. Tanwar, R. Parui, R. Garai, M. A. Chanu and P. K. Iyer, *ACS Meas. Sci. Au*, 2021, **2**, 23–30.

 This journal is © The Royal Society of Chemistry 2024